IEEE Access
Multidisciplinary | Rapid Review | Open Access Journal

Received 6 December 2023, accepted 6 January 2024, date of publication 10 January 2024,
date of current version 19 January 2024.

Digital Object Identifier 10.1109/ACCESS.2024.3352449

RESEARCH ARTICLE

An Optimized Ka-Band Low Profile Dual-Polarized Transmitarray Antenna With 2D Beam Switching

SEYED HASHEM RAMAZANNIA TULOTI, ADAM LAMECKI, (Senior Member, IEEE), AND MICHAL MROZOWSKI, (Fellow, IEEE)
Faculty of Electronics, Telecommunications, and Informatics, Gdańsk University of Technology, 80-233 Gdańsk, Poland

Corresponding author: Seyed Hashem Ramazannia Tuloti (h.ramazannia@pg.edu.pl)

This work was supported by the Polish National Science Centre under Contract UMO-2019/33/B/ST7/00889.

ABSTRACT This article presents an optimized dual-polarized transmitarray antenna (TA) designed for MIMO applications at the Ka-band, capable of switching beams in two directions. The antenna aperture uses a small unit cell with three layers of Taconic RF-35 dielectric substrates, which can be easily fabricated using PCB technology. The unit cell achieved a 360-degree phase shift and a transmission magnitude exceeding –0.4 dB at 28 GHz. We used nine dual-polarized patch antennas in a cross shape, each with a 10.5 dBi gain at 28 GHz, to switch the beams in two directions without changing the feed location. We optimized the phase distribution in the TA aperture and adjusted the feed antenna's F/D and tilt to achieve a high-gain antenna with low-gain roll-off during beam switching. The fabricated TA exhibited excellent agreement with the full-wave simulation results. It achieved ± 15 degrees and ± 30 degrees beam tilts in the x- and y- directions, with less than 0.8 dB gain roll-off for both polarizations.

INDEX TERMS Transmitarray antennas, 2D beam switching, low profile, dual-polarized, gain roll-off.

I. INTRODUCTION

High-gain and beam-scanning antennas are critical to modern millimeter-wave communication applications [1]. Transmitarray antennas (TA) take advantage of both optical theory and antenna array techniques to attain a low-profile, high-radiation, efficient design suitable for various wireless communication systems. [2].

Dual-polarization in TAs is typically achieved by applying multilayer frequency selective surfaces (M-FSS) [3], [4], [5], or the receive-transmit (R-T) scheme [6], [7]. TAs can perform beam scanning using either electrical or mechanical control solutions. In the case of electrical control, RF components such as PIN diodes are added to each unit cell to achieve tunable transmission phases by controlling the DC bias [8], [9], [10], [11]. However, this approach is expensive, lossy, and complex. Passive TAs, on the other hand, can only provide a fixed phase shift once their dimensions are determined. Nevertheless, the beams of the passive TAs can be mechanically steered by moving the feed source [12], [13], [14], [15], [16], [17], [18], [19], which causes a high gain roll-off issue. This occurs when the feed source veers from the center to scan the beams in a unifocal TA with an aperture designed for the center-located feed source. A possible solution is to use multifocal TAs to adjust the phase distribution within the TA apertures [20]. This reduces the high gain roll-off but comes at the cost of lowering the overall gains of the antennas. Usually, horn antennas are employed to illuminate TAs due to their superior gain and efficiency (Fig. 1(a)); however, they possess a high profile.

This paper proposes a novel design for a high-efficiency, low-profile, dual-polarized TA with beam-switching

The associate editor coordinating the review of this manuscript and approving it for publication was Derek Abbott.

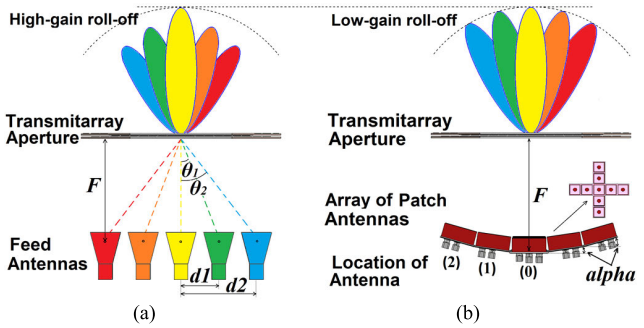

FIGURE 1. Beam-steerable TA: (a) the feed source is mechanically moved along a straight line, and (b) the proposed TA using multiple feed sources.

capabilities and low gain roll-off. The antenna aperture consists of an M-FSS with a wideband passband unit cell smaller than previously reported unit cells of the same frequency. The unit cell provides a 360-degree phase shift at 28 GHz with a magnitude loss exceeding 0.4 dB. The TA comprises nine dual-polarized patch antennas arranged in a cross shape (Fig. 1(b)) as a switchable feed to illuminate the aperture for achieving 2D beam-steering capability and a low profile. The phase distribution in the unifocal TA aperture has been optimized to reduce the beam-scanning gain roll-off and prevent lowering the final gain of the TA; the value of F has been adjusted to reduce the effects of orthogonal incident estimation, and the tilt of the feed antennas has been adjusted to minimize spillover loss. The optimized antenna performs better and has a lower profile than similar Ka-Band scanning/switching TAs reported until.

This paper is organized as follows: Section II presents a compact and low-loss dual-polarized unit cell with small dimensions ($0.28\lambda \times 0.28\lambda$ at 28 GHz); Section III details a 28 GHz patch antenna that serves as a feed for the transmitarray aperture; Section IV describes optimizing a TA employing nine patch antennas in a cross shape to achieve 2D beam switching and; Section V concludes the paper.

II. LOW-LOSS, DUAL-POLARIZED UNIT-CELL

The beam-focusing aperture, consisting of unit cells, is a critical component of a TA. Different types of unit cells can be used in a TA, depending on bandwidth, polarization, design, and manufacturing constraints. The dimensions of the unit cells determine the spacing between cells and the number of unit cells required on the aperture of the TA. For a TA to perform well, the unit cell must be designed to provide a 360-degree phase shift in the transmit phase while maintaining a transmit amplitude close to 1 (0 dB) [21].

Fig. 2 represents the configuration, parameters, and simulated transmission coefficients of the unit cell used in this paper. It consists of a pair of three-layer stacked Taconic RF-35 dielectric substrates (with permittivity, $\varepsilon_r = 3.43$, dielectric loss tangent, $\tan\delta = 0.0018$, and thickness = 0.254 mm) separated by a 2.5 mm air gap, as illustrated in Fig. 2(a). The unit cell has two circular patches in the top and bottom layers and a circular ring with four lines in

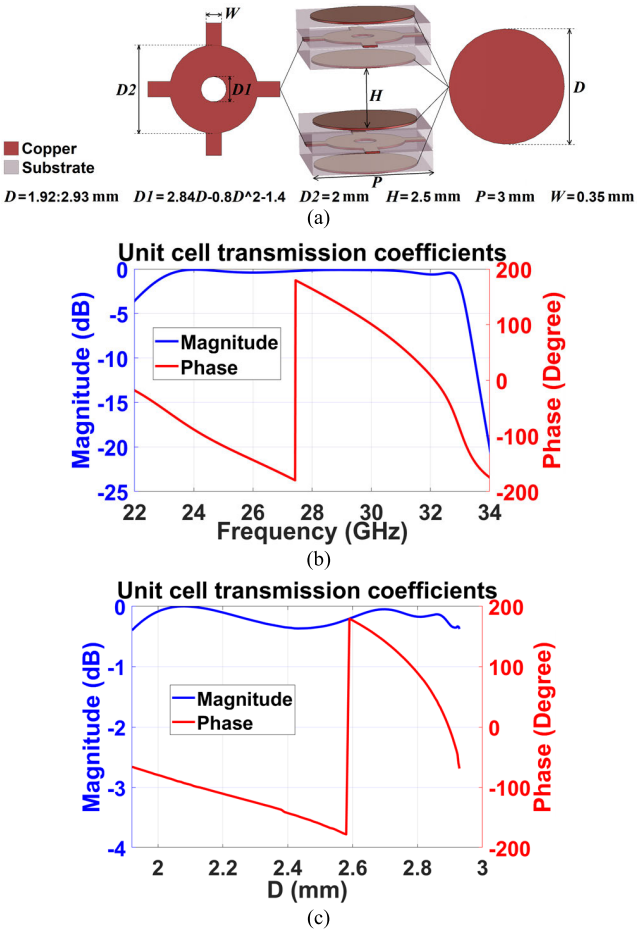

FIGURE 2. Unit cell: (a) configuration and parameters, (b) transmission coefficients in terms of frequency (D = 2.6mm), and (c) transmission coefficients in terms of D parameter at 28 GHz (D is swept from 1.92 to 2.93 mm).

the middle layer of each stacked FSS. The unit cell can be easily fabricated using PCB technology and is suitable for dual polarization applications due to its symmetry. We modified the design from [22], where a transmission phase of 250 degrees was obtained, by changing the square patches and rings to circular ones and adjusting the inner diameter of the circular ring in the middle layer ($D1$) as inversely proportional to the circular patch diameter (D), as depicted in the figure. This enabled us to achieve a relatively higher transmission phase of 360 degrees. We employed CST Microwave Studio software [23] to simulate the transmission coefficients of the unit cell by applying periodic boundary conditions and radiating a plane wave from top to bottom. The results for a fixed circular patch diameter of 2.6 mm and varying D at 28 GHz are illustrated in Figs. 2(b) and 2(c), respectively. By changing D from 1.92 mm to 2.93 mm, we achieved the required phase shift at 28 GHz with less than 0.4 dB transmission magnitude loss. This allowed us to design a highly efficient wideband TA and optimize the antenna aperture for beam scanning. The unit cell in this design is smaller than the ones examined in the literature, which reduces the sidelobe levels in the TA by fitting more unit cells into the aperture.

To verify the performance of the unit cell, a TA antenna, which consists of 381 cells, was simulated using CST Microwave Studio software. The focal length (F), which is the distance between the feed antenna and the TA aperture, is 30 mm ($F/D = 0.4$, where D is the largest dimension of the antenna surface). An axial corrugated conical horn antenna with a gain of 11.5 dBi at 28 GHz is used as the feed. Fig. 3 shows the radiation patterns of the antenna. The maximum gain of the antenna at 28 GHz is 24 dBi, and the aperture efficiency at the same frequency is 67%. The antenna has a wide gain bandwidth, and the first sidelobe level is −33 dB and −29 dB in the E- and H-planes, respectively.

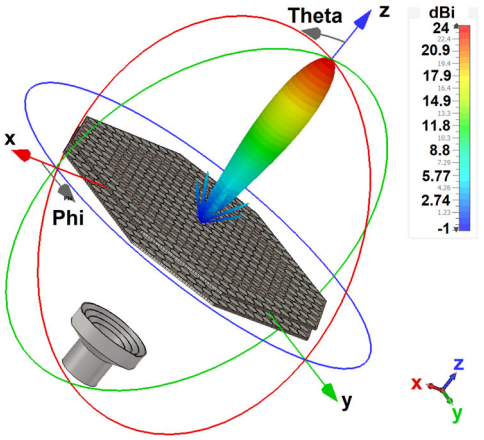

FIGURE 3. A simulated TA antenna to verify the performance of the unit cell.

III. DUAL-POLARIZED PATCH ANTENNA AS FEED

Fig. 4(a) presents the configuration of the circular microstrip patch antenna designed to illuminate the TA aperture. To achieve a dual-polarization operation, the patch is fed through two U-shaped slots in the center ground plane [24], [25], [26]. The antenna uses a Taconic RF-TLY-5 dielectric substrate (with $\varepsilon_r = 2.2$, $\tan\delta = 0.001$), with a thickness of 0.254 mm on the patch side and 0.127 mm on the feed microstrip side, where SMPS-type connectors are provided. In addition, a square metal reflector with dimensions of 10 mm and a height of 4.5 mm is used to increase the gain of the patch antenna, resulting in an increased gain of about 2.8 dB. It also augmented the bandwidth of the antenna. The patch antenna size, the dimensions of the U-shaped slots in the ground plane, their distance from the patch center, the feeding microstrip lines on the bottom layer, and their offset from the patch center are optimized to improve the antenna performance. The fabricated antenna is represented in Fig. 4(b); its measured and simulated S-parameters and radiation patterns are depicted in Figs. 4(c) and 4(d), respectively. The simulated and measured values agree well, and the antenna achieves a gain of 10.5 dBi at 28 GHz. A small shift in the operating frequency band and some ripple in the measured S-parameter plot may be due to manufacturing errors and calibration issues, respectively. The network analyzer was calibrated using a 2.9-type connector; however, a 6-inch conversion cable was used to connect to the antenna, which was not accounted for in the calibration. It should be noted that the loss of this cable is considered in the measurement results.

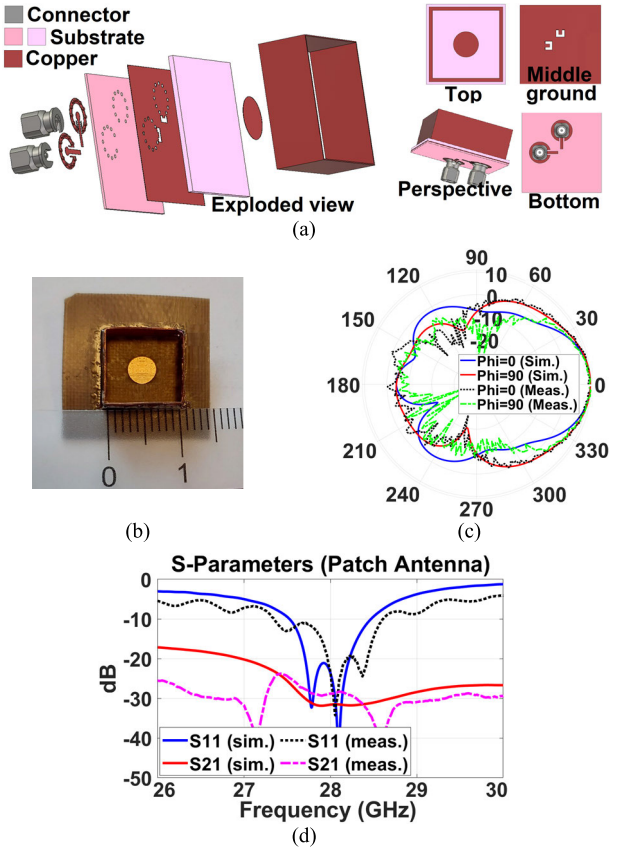

FIGURE 4. Feeding patch antenna: (a) configuration of antenna, (b) fabricated antenna, (c) simulated and measured S-parameters for the proposed patch antenna, and (d) measured and simulated radiation patterns at E-plane and H-plane at 28 GHz.

IV. BEAM-STEERABLE TRANSMITARRAY ANTENNA

Based on the results presented in Sections II and III, we designed and optimized a TA for 28 GHz that can switch the beams by ±15 degrees and ±30 degrees in both the x- and y-directions. The TA aperture contains 381 unit cells from Section II. We used nine patch antennas in a cross-shape layout as feed to achieve two-dimensional beam switching (Fig. 1(b)). As shown, one patch antenna at position (0) produces a broadside beam, and four patch antennas at position (1) in the +x, –x, +y, and –y directions result in the main beam being deflected by about 15 degrees. In addition, four patch antennas are located at position (2) in the +x, –x, +y, and –y directions, causing the main beam to tilt about 30 degrees.

To achieve a low-profile antenna, we initially used $F/D = 0.4$. This initial parameter will be optimized later. To reduce spillover loss and gain reduction at high scan angles, we initially tilted the feed at each location toward the center of the TA aperture. We will optimize this value later as well. To achieve a suitable gain roll-off, we implemented these measures in the antenna design:

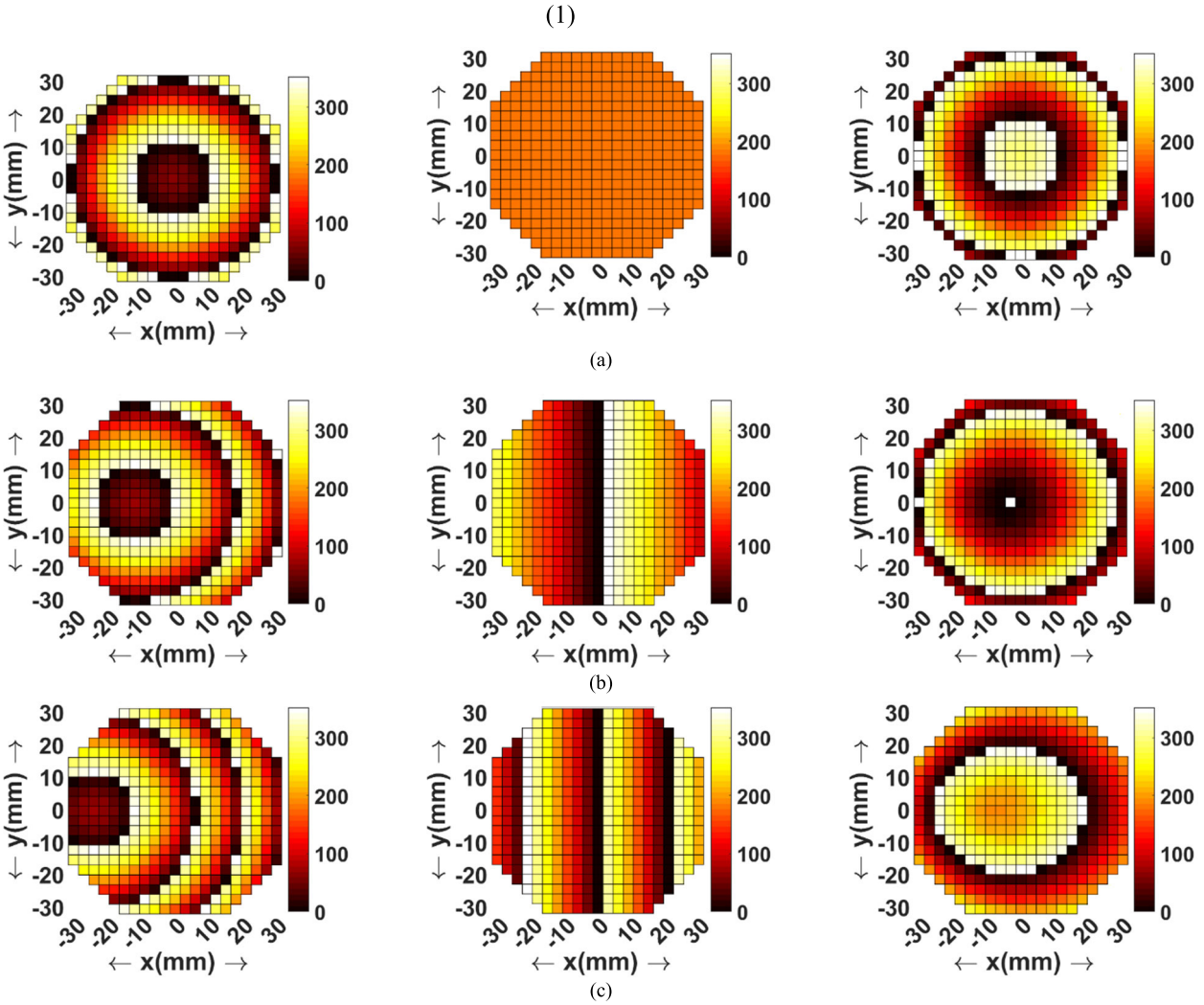

FIGURE 5. Phase distribution on TA aperture ($\psi_0 = 0$): (a) for broadside main beam when feed antenna located at positions (0), (b) for main beam tilted 15 degrees when feed antenna located at positions (1) and (c) for main beam tilted 30 degrees when feed antenna located at positions (2).

A. Optimizing the phase distribution in the TA aperture

B. Optimizing F/D, and Optimizing the feed antenna tilt

In this study, all simulations were executed using CST Microwave Studio Software. The computational parameters utilized consisted of the Time Domain Solver, employing a Hexahedral mesh type with an accuracy of −40 dB, 20 cells per wavelength, and 25 cells per maximum model box edge, ensuring sufficient simulation precision. The simulations were conducted on a computer with a 64-bit operating system with Intel(R) Xeon(R) Gold 6136 CPU processor and 576 GB RAM. Each simulation run, encompassing the entire structure, took approximately 23 hours and consumed 30.2 GB of memory.

A. OPTIMIZING THE PHASE DISTRIBUTION IN THE TA APERTURE

Based on the space-fed TA structure, the required transmission phase for each unit cell, which compensates for the phase delay of the feed to that cell to create a specified phase distribution for beam concentration in a given direction, is calculated as follows:

$$\psi_{ij} = k\left(R_{ij} - \vec{r}_{ij}.\hat{\boldsymbol{r}}_{\mathbf{0}}\right) + \psi_0 \tag{1}$$

where ψ_{ij} is the required transmission phase for the ijth unit cell, k is the propagation constant in free space, R_{ij} is the distance from the phase center of feed to the ijth cell, $\vec{r}_{ij}$ is the position vector of the ijth unit cell, the main beam unit vector is presented by $\hat{\boldsymbol{r}}_{\mathbf{0}}$, and, ψ_0 is a constant phase.

Because the unit cell typically does not cover the full 360-degree range, the value of ψ_0 is selected to ensure the required phase for the central cells, where the feed's radiation concentration is higher, falls within the range where the unit cell exhibits suitable transmission magnitude. This approach has been adopted to prevent a reduction in the final gain of the TA. In the case of the unit cell discussed in this article, as it has achieved a full 360-degree transition phase with a transmission magnitude exceeding –0.4 dB, any value for ψ_0 can be considered, with no concern about reducing the gain.

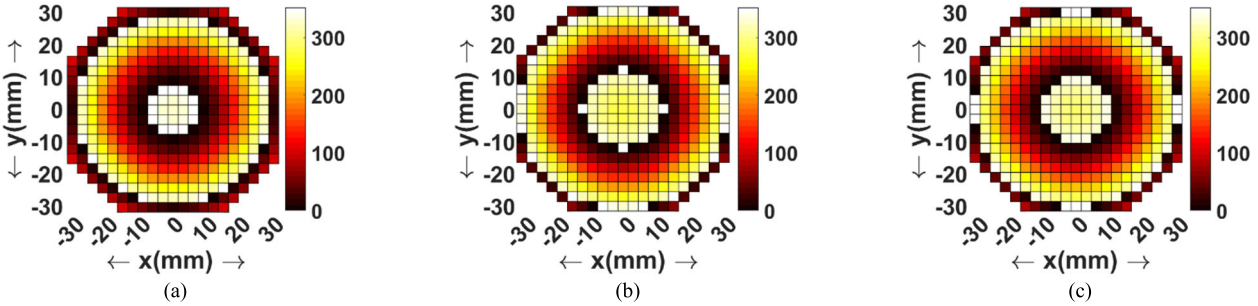

FIGURE 6. The optimized phase distribution on TA: (a) Δ_{15} has been optimized, (b) Δ_{30} has been optimized and (c) $\Delta_{15}+\Delta_{30}$ has been optimized.

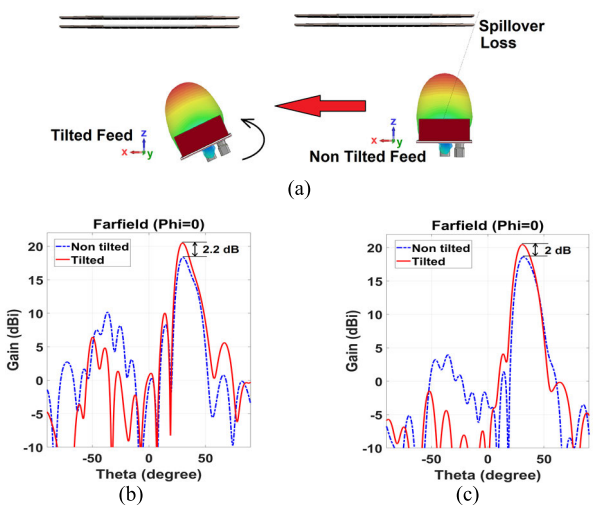

FIGURE 7. Effect of spillover loss: (a) schematic of tilting the feed toward the center of transmitarray aperture, and radiation pattern for tilted and non-tilted patch antenna at location (2) in the -x direction at 28 GHz: (b) H-plane for y-polarization and (c) E-plane for x-polarization.

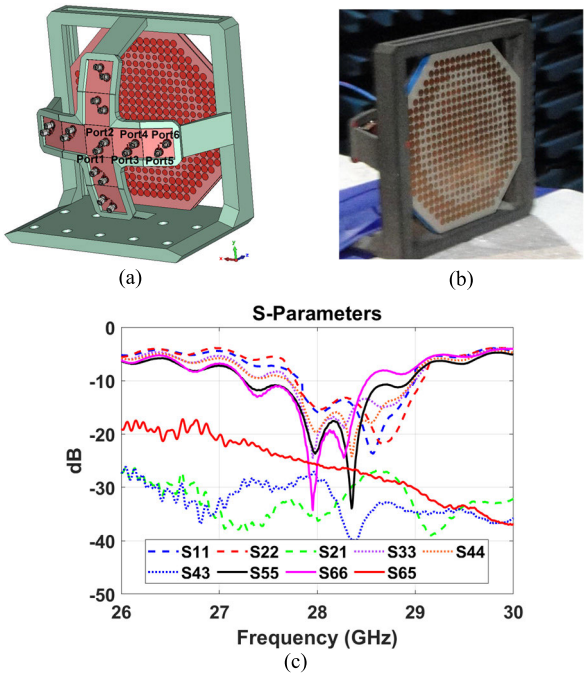

FIGURE 8. Purposed TA: (a) schematic of antenna, (b) Fabricated TA, (c) Measured S-parameters.

This allows us to explore the optimization of the TA aperture to reduce the gain roll-off during high beam switching.

Fig. 5 depicts the phase distribution on the TA aperture in three different cases. Fig. 5(a) shows the feed antenna positioned at (0), resulting in a TA with a broadside main beam. Fig. 5(b) represents a main beam tilted at 15 degrees when the feed antenna is located at position (1). Finally, Fig. 5(c) illustrates the feed antenna at position (2), resulting in a main beam tilted at 30 degrees. Each case consists of three plots: the first plot illustrates the phase received by each unit cell from the feed antenna; the second represents the final required phase distribution necessary to achieve the desired main beam direction and; the third displays the required transmission phase for each element when $\psi_0 = 0$, progressing from left to right.

The objective of the optimization process is to determine the appropriate value of ψ_0 for case (a) that minimizes the sum of the phase differences between cells in case (a) and case (b) + (c). To achieve this, a constant phase was added to each case so that the required transmission phase of the central cell becomes zero ($\psi_{ij}(a_0)$, $\psi_{ij}(b_0)$ and $\psi_{ij}(c_0)$). Equations (2) and (3) were then utilized to calculate the optimal value of ψ_0. The obtained optimal values were 335 degrees for Δ_{15} (tilt of 15 degrees) and 278 degrees for Δ_{30} (tilt of 30 degrees). When the sum of Δ_{15} and Δ_{30} was minimized, the value of ψ_0 was determined to be 297 degrees. These results are presented in Fig. 6.

$$\Delta_{15} = \sum_{i=0}^{N} \sum_{j=0}^{N} \left| \psi_{ij}(a_0) + \psi_0 - \psi_{ij}(b_0) \right| \quad (2)$$

$$\Delta_{30} = \sum_{i=0}^{N} \sum_{j=0}^{N} \left| \psi_{ij}(a_0) + \psi_0 - \psi_{ij}(c_0) \right| \quad (3)$$

B. OPTIMIZING THE VALUES OF F/D AND TILT OF FEED ANTENNAS

In this stage, the goal is to optimize F and alpha, depicted in Fig. 1(b), for maximum gain and minimum gain roll-off when switching the beam. For this purpose, the antenna aperture in Fig. 6(c) was used, with initial values of $F/D = 0.4$ and alpha $= 11.3$ degrees. By performing several full-wave simulations with CST Microwave Studio software and tuning

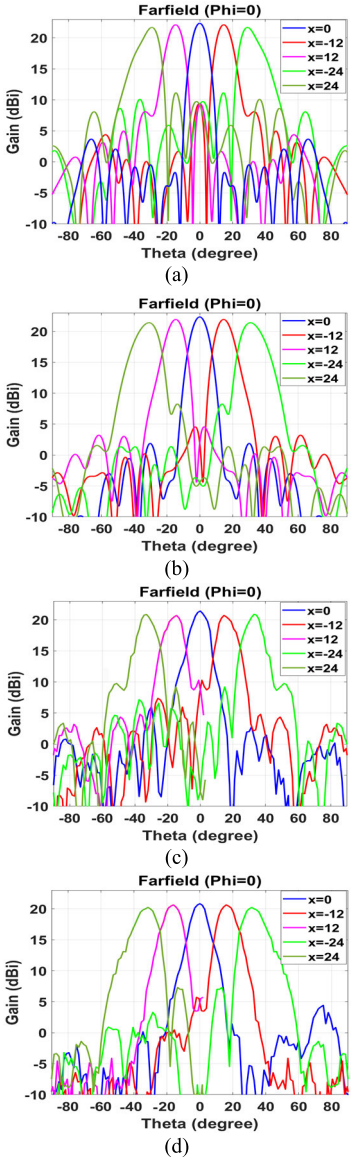

FIGURE 9. Radiation patterns of purposed TA: (a) simulated radiation pattern, H-plane for y-polarization at 28 GHz, (b) simulated radiation pattern, E-plane for x-polarization at 28 GHz, (c) measured radiation pattern, H-plane for y-polarization at 28 GHz and (d) measured radiation pattern, E-plane for x-polarization at 28 GHz.

F and alpha, the optimal values of 0.42 and 10.1 were determined.

Using Fig. 2(c) to determine the required phase for cells (in the presence of an orthogonal incident wave) results in variations as a cell moves away from the aperture's center and the incident angle increases. These deviations from the ideal orthogonal conditions cause a reduction in gain. A slight modification was made to the F/D value to address the influence of oblique incident angles.

To reduce spillover loss and counter the decrease in gain at high scan angles, we initially implemented a tilt to the feed at each position, directing it towards the center of the TA aperture (Fig. 7(a)). Fig. 7(b) and Fig. 7(c) show the radiation pattern for tilted and non-tilted patch antennas at position (2) in the -x direction, in the H-plane for y-polarization and

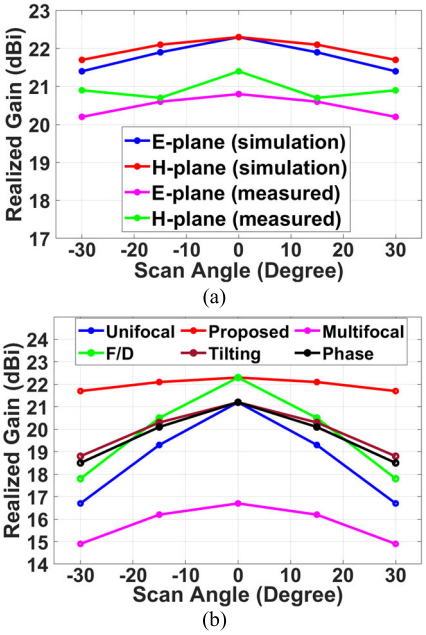

FIGURE 10. Realized gain of the TA with different scan angles at 28 GHz: (a) Fabricated TA and (b) The impact of each optimization component.

E-plane for x-polarization, respectively, at 28 GHz. It can be seen that tilting the patch antenna results in an increase of more than 2 dB in the total gain of the TA. Nevertheless, given the antenna structure's characteristics and the patch antenna's radiation pattern, this angle may not always be the most suitable option. We carefully adjusted the angle to enhance this parameter to achieve maximum gain.

Figs. 8 and 9 record these results, indicating the highest gain and the lowest gain roll-off during beam switching. Fig. 9(b) displays the simulated realized gain for the unifocal, multifocal, and proposed TAs at 28 GHz based on varying scan angles. Additionally, it visualizes the impact of individual optimization components on the unifocal TA.

C. FABRICATING AND TESTING THE DESIGNED ANTENNA

The designed TA and the fabricated antenna with cross-shaped feeding patches are represented in Figs. 8(a) and 8(b). In Fig. 8(c), the measured S-parameters of the antenna are depicted, revealing satisfactory matching at 28 GHz. The observed ripple in the S-parameter plot may be attributed to calibration issues. Additionally, variations among the results from different ports could arise from potential manufacturing errors, as the ports are manually soldered.

The antenna has dual polarization and can scan its main beam in both x- and y-directions. Fig. 9 compares the simulated and measured beam tilting in the x-direction for x- and y-polarizations. The results for the y-direction are identical due to the antenna's symmetry. Figs. 9(a) and 9(b) illustrate that the antenna performs better in y-polarization for gain roll-off and in x-polarization for sidelobe level, which is related to the patch antenna pattern asymmetry (see Fig. 4(d)). Figs. 9(c) and 9(d) also show the measured radiation pattern

TABLE 1. Comparison of the proposed TA with some references in beam-scanning antennas.

Ref.	Freq. [GHz]	Unit cell						Transmitarray						
		Size [λ_0^2]	Thickness	Phase Range	Loss [dB]	Type	Polarization	Feed Antenna(s)	Beam Scanning Technology	Beam-Scanning	Scan Range	Gain [dBi]	Aperture Efficiency	Gain roll-off
[12]	30	0.49	$4\lambda_0$	270°	1.25	Waveguide	Dual	Horn	Moving the feed	2D	$\pm 18^\circ$	28.8	41.9%	2/4 dB
[13]	27	0.2025	$0.373\lambda_0$	270°	0.9	R-T	Circular	Dipole	Selecting the feed	1D	$\pm 33^\circ$	18.5	24.8%	2 dB
[14]	25	0.1736	$0.67\lambda_0$	360°	1.1	M-FSS	Dual	Horn	Moving the feed	1D	$\pm 30^\circ$	29.4	25%	1.6 dB
[16]	30	0.09	$3.3\lambda_0$	360°	2.4	Waveguide	Dual	Horn	Moving the feed	1D	$\pm 27^\circ$	30	35.1%	2.9 dB
[17]	28.5	0.3025	$0.576\lambda_0$	300°	1	M-FSS	Circular	Patch	Selecting the feed	1D	$\pm 30^\circ$	25	32.3%	3.5 dB
[18]	28	0.0484	$0.14\lambda_0$	$0, 180^\circ$	1.5	M-FSS	Linear	Yagi	Selecting the feed	2D	$\pm 15^\circ$	19.7	23.6%	1.6 dB
[19]	26	0.4133	$10.1\lambda_0$	315°	0.35	Waveguide	Dual	Horn	Moving the feed	2D	$\pm 28^\circ$	30.3	45.1%	4.5 dB
This study	28	0.0784	$0.336\lambda_0$	360°	0.4	M-FSS	Dual	Patch	Selecting the feed	2D	$\pm 30^\circ$	21.4	36.8%	0.7/0.8 dB

of the antenna at 28 GHz for y- and x-polarizations (H- and E-planes), respectively, which agree well with the simulations. A small discrepancy of about 1 dB is observed, which may be caused by fabrication, assembly, or measurement errors.

Fig. 10(a) plots the realized gain of the TA at 28 GHz for H- and E-planes for both simulations and measurements as a function of scan angle. The results ascertain that the measured gains roll-off are only 0.8 and 0.7 dB for the H- and E-planes, respectively. In Fig. 10(b), the realized gain of the TA antenna at 28 GHz is presented for various scan angles. The red plot represents the final proposed optimized antenna, while the blue and pink plots depict the unifocal (without optimization) and multifocal designs, respectively. The figure also shows the individual impact of optimization components. The green plot, corresponding to the optimization of F/D, demonstrates a consistent improvement in antenna efficiency without affecting gain roll-off across different scan angles (approximately 1.2 dB). In comparison to the unifocal design, both feed tilting and phase optimization (brown and black graphs) contributed similarly to gain increase (around 1 dB for a 15° scan and approximately 2 dB for a 30° scan), with a slightly greater effect observed for feed tilting. The proposed antenna results from the integration of all optimization components into the design.

Table 1 compares the proposed TA with similar beam-scanning antennas from the literature. The aperture efficiency η_{ap} in the table is calculated using:

$$\eta_{ap} = \frac{G}{D_{max}}, \quad D_{max} = \frac{4\pi A}{\lambda_0^2} \tag{4}$$

where G is the measured gain, D_{max} is the maximum directivity, A is the area of the antenna aperture, and λ_0 is the free-space wavelength.

A few conclusions can be drawn based on the data provided in Table 1. First, considering the unit cell size and the phase range achieved (the columns in the left part of the table), the unit cell in our design is very small and yet it provides a complete 360° phase with only a 0.4 dB loss. In fact, it is the second-smallest unit cell in all antennas compared in the table, but with lower loss and complete phase range. This demonstrates the high efficiency and compactness of our antenna. Second, concerning the TA feeding antenna, unlike some antennas that use horn antennas, we employ patch antennas and this gives us a low-profile design. Among antennas without horn antennas, ours stands out as the most efficient and capable of scanning beams in 2D. Note that our primary objective was to achieve low gain roll-off, even at high scanning angles, while maintaining high efficiency. This came at a cost of smaller gain than in references [16], [17], and [19]. Indeed, all antennas in the table with higher gain than ours, i.e. [16], [17], and [19], suffer from significant gain roll-off. Our optimization method can also be used for antennas with higher gain, especially those for which the gain roll-off issue is important.

V. CONCLUSION

We designed a low-profile, high-efficiency dual-polarized transmitarray antenna for 28 GHz MIMO applications with two-dimensional beam switching. The antenna comprises an aperture of 381 low-loss, dual-polarized unit cells and a cross-shaped array of dual-polarized patch antennas as feed. By optimizing the phase, F/D, and the tilt of the feed antennas, we achieved ±15 degrees and ±30 degrees beam switches in both x- and y-directions with less than 0.8 dB gain roll-off by selecting the feed patch antenna in both polarizations.

REFERENCES

[1] S. Ghosh and D. Sen, "An inclusive survey on array antenna design for millimeter-wave communications," *IEEE Access*, vol. 7, pp. 83137–83161, 2019.

[2] S. H. R. Tuloti, P. Rezaei, and F. T. Hamedani, "High-efficient wideband transmitarray antenna," *IEEE Antennas Wireless Propag. Lett.*, vol. 17, no. 5, pp. 817–820, May 2018.

[3] A. Aziz, F. Yang, S. Xu, M. Li, and H.-T. Chen, "A high-gain dual-band and dual-polarized transmitarray using novel loop elements," *IEEE Antennas Wireless Propag. Lett.*, vol. 18, no. 6, pp. 1213–1217, Jun. 2019.

[4] S. Yang, Z. Yan, T. Zhang, M. Cai, F. Fan, and X. Li, "Multifunctional tri-band dual-polarized antenna combining transmitarray and reflectarray," *IEEE Trans. Antennas Propag.*, vol. 69, no. 9, pp. 6016–6021, Sep. 2021.

[5] S. H. Ramazannia Tuloti, Z. Mousavirazi, A. Kesavan, and T. A. Denidni, "A low profile dual-polarized transmitarray antenna at Ka-band," *AEU-Int. J. Electron. Commun.*, vol. 143, Jan. 2022, Art. no. 154016.

[6] F. Wu, J. Wang, L. Xiang, W. Hong, and K.-M. Luk, "A wideband dual-polarized magneto-electric dipole transmitarray with independent control of polarizations," *IEEE Trans. Antennas Propag.*, vol. 70, no. 9, pp. 8632–8636, Sep. 2022.

[7] Y. Wang, S. Xu, F. Yang, and D. H. Werner, "1 bit dual-linear polarized reconfigurable transmitarray antenna using asymmetric dipole elements with parasitic bypass dipoles," *IEEE Trans. Antennas Propag.*, vol. 69, no. 2, pp. 1188–1192, Feb. 2021.
[8] X. Wang, P.-Y. Qin, A. Tuyen Le, H. Zhang, R. Jin, and Y. J. Guo, "Beam scanning transmitarray employing reconfigurable dual-layer Huygens element," *IEEE Trans. Antennas Propag.*, vol. 70, no. 9, pp. 7491–7500, Sep. 2022.
[9] C.-W. Luo, G. Zhao, Y.-C. Jiao, G.-T. Chen, and Y.-D. Yan, "Wideband 1 bit reconfigurable transmitarray antenna based on polarization rotation element," *IEEE Antennas Wireless Propag. Lett.*, vol. 20, no. 5, pp. 798–802, May 2021.
[10] T.-J. Li, G.-M. Wang, W.-L. Guo, K.-W. Xin, J.-Q. Han, and H.-P. Li, "Reconfigurable folded transmitarray antenna with low-profile based on metasurfaces," *IEEE Antennas Wireless Propag. Lett.*, vol. 22, no. 3, pp. 611–615, Mar. 2023.
[11] J. Tang, S. Xu, F. Yang, and M. Li, "Design and measurement of a reconfigurable transmitarray antenna with compact varactor-based phase shifters," *IEEE Antennas Wireless Propag. Lett.*, vol. 20, no. 10, pp. 1998–2002, Oct. 2021.
[12] X. Wang, Y. Cheng, and Y. Dong, "Millimeter-wave dual-polarized metal transmitarray antenna with wide gain bandwidth," *IEEE Antennas Wireless Propag. Lett.*, vol. 21, no. 2, pp. 381–385, Feb. 2022.
[13] J. Hu, H. Wong, and L. Ge, "A circularly-polarized multi-beam magneto-electric dipole transmitarray with linearly-polarized feeds for millimeter-wave applications," *IEEE Trans. Antennas Propag.*, vol. 70, no. 7, pp. 6012–6017, Jul. 2022.
[14] P. Mei, G. F. Pedersen, and S. Zhang, "Performance improvement of mechanically beam-steerable transmitarray antennas by using offset unifocal phase symmetry," *IEEE Trans. Antennas Propag.*, vol. 71, no. 1, pp. 1129–1134, Jan. 2023.
[15] A. Papathanasopoulos and Y. Rahmat-Samii, "Transmitarray antenna for conical beam scanning," *IEEE Trans. Antennas Propag.*, vol. 70, no. 11, pp. 11155–11160, Nov. 2022.
[16] A. Massaccesi, G. Dassano, and P. Pirinoli, "Beam scanning capabilities of a 3D-printed perforated dielectric transmitarray," *Electronics*, vol. 8, no. 4, p. 379, Mar. 2019.
[17] G. Liu, M. R. Dehghani Kodnoeih, K. T. Pham, E. M. Cruz, D. González-Ovejero, and R. Sauleau, "A millimeter-wave multibeam transparent transmitarray antenna at Ka-band," *IEEE Antennas Wireless Propag. Lett.*, vol. 18, no. 4, pp. 631–635, Apr. 2019.
[18] J. A. Ganie and K. Saurav, "Two-dimensional switchable beam transmitarray antenna for mm-wave base stations and vehicular networks," *IEEE Access*, vol. 11, pp. 34563–34574, 2023.
[19] Y. Cao, W. Wu, S. Wu, J. Li, and S. Yan, "Cavity-filter-based 3-D-printed gain-filtering transmitarray for multibeam applications," *IEEE Trans. Antennas Propag.*, vol. 71, no. 12, pp. 9685–9695, Dec. 2023, doi: 10.1109/TAP.2023.3323785.
[20] F. Qin, R. Song, W. Cheng, and H. Zhang, "Multibeam OAM transmitarray with stable vortex property based on bifocal method," *IEEE Antennas Wireless Propag. Lett.*, vol. 20, no. 9, pp. 1601–1605, Sep. 2021.
[21] A. H. Abdelrahman, F. Yang, A. Z. Elsherbeni, and P. Nayeri, "Analysis and design of transmitarray antennas," *Synth. Lectures Antennas*, vol. 6, no. 1, pp. 1–175, Jan. 2017.
[22] Q. Luo, S. Gao, M. Sobhy, and X. Yang, "Wideband transmitarray with reduced profile," *IEEE Antennas Wireless Propag. Lett.*, vol. 17, no. 3, pp. 450–453, Mar. 2018.
[23] Dassault Systèmes, Vélizy-Villacoublay, France. (Jun. 3, 2022). *CST Microwave Studio. Release Version 2022.05*. [Online]. Available: http://www.cst.com
[24] T. H. Jang, H. Y. Kim, D. M. Kang, S. H. Kim, and C. S. Park, "60 GHz low-profile, wideband dual-polarized U-slot coupled patch antenna with high isolation," *IEEE Trans. Antennas Propag.*, vol. 67, no. 7, pp. 4453–4462, Jul. 2019.
[25] X. Yang, N. Zhu, N. Xie, M. Hou, and S. Gao, "Broadband dual-polarized phased array with broadside and endfire radiation for 5G millimeter wave communications," in *Proc. Comput., Commun. IoT Appl. (ComComAp)*, Oct. 2019, pp. 210–212.
[26] K. Trzebiatowski, W. Kalista, M. Rzymowski, L. Kulas, and K. Nyka, "Multibeam antenna for Ka-band CubeSat connectivity using 3-D printed lens and antenna array," *IEEE Antennas Wireless Propag. Lett.*, vol. 21, no. 11, pp. 2244–2248, Nov. 2022.

SEYED HASHEM RAMAZANNIA TULOTI was born in Babol, Iran, in 1987. He received the B.Sc. degree in electronic engineering from the Babol Noshirvani University of Technology, Babol, in 2010, the M.Sc. degree in wave and field telecommunication engineering from the K. N. Toosi University of Technology, Tehran, Iran, in 2013, and the Ph.D. degree in field telecommunication engineering from the University of Semnan, Semnan, Iran, in 2019. He joined to the Gdańsk University of Technology as a Research Assistant Professor. Also, he has more than seven years of working experience as the Manager of Research and Development at a factory manufacturing RF components. His research interests include antennas, transmitarray antennas, reconfigurable RF components for future RF systems, phase array antennas, mm-wave applications, and passive RF components.

ADAM LAMECKI (Senior Member, IEEE) received the M.S.E.E. and Ph.D. degrees in microwave engineering from the Gdańsk University of Technology (GUT), Gdańsk, Poland, in 2002 and 2007, respectively. In 2007, he cofounded EM Invent, Gdańsk, a spin-off company, which develops an electromagnetic field simulator InventSim, where he was the Chief Technology Officer (CTO). Since 2019, he has been an Associate Professor with the Department of Microwave and Antenna Engineering, GUT. His research interests include filter design and optimization techniques, surrogate models and their application to the computer-aided design (CAD) of microwave devices, and computational electromagnetics (mainly focused on the finite-element method).

MICHAL MROZOWSKI (Fellow, IEEE) received the M.Sc. degree (Hons.) in telecommunication engineering and the Ph.D. degree (Hons.) in electronic engineering from the Gdańsk University of Technology (GUT), in 1983 and 1990, respectively. In 1986, he joined the Department of Electronics, GUT, where he is currently a Full Professor, the Head of the Department of Microwave and Antenna Engineering, and the Director of the Doctoral School. He has developed several software modules that have been then integrated into commercial microwave EDA software used all over the world. He has published one book and over 100 peer-reviewed articles in IEEE journals. His research interests include computational electromagnetics, photonics, and microwave engineering. His current work is focused on the development of new fast numerical techniques for solving 2D and 3D boundary value problems in the time and frequency domains, automated microwave filter design, microwave filter synthesis, microwave sensor design, microwave EDA, reduced-order models for grid-based numerical techniques (e.g., FDTD and FEM), and surrogate model construction.

He also serves as a member of the Editorial Board for IEEE Access. He is a member of the MTT-1 and MTT-2 Technical Committees, a fellow of the Electromagnetics Academy, and a member of the Polish Academy of Sciences. Furthermore, he is the past Vice-Dean of Research of the ETI Faculty and the past Chairperson of the Polish AES/AP/MTT Chapter. He served as an Associate Editor for IEEE Microwave and Wireless Components Letters and a member of the Editorial Board for the Proceedings of the IEEE.